Supplementary information for

Triple-Junction Optoelectronic Sensor with Nanophotonic Layer Integration for Single Molecule Level Decoding

Hsin-Yi Hsieh*, Yu-Hsuan Peng, Sheng-Fu Lin, Li-Ching Chen, Teng-Chien Yu, Chung-Fan Chiou, Johnsee Lee
Personal Genomics, Inc., Hsinchu Biomedical Science Park, Zhubei, Hsinchu 30261, Taiwan.
*email: hyhsieh@personalgx.com

1. Nanophotonic layer (NPL) fabrication process
2. NPL design principle
3. Filters on TPD CMOS
4. Photon collection after the pinhole

1. NPL fabrication process

The received 8" CMOS wafers with a triple-junction photodiode (TPD) designed in-house and fabricated with a 0.18-μm CMOS image sensor by the 4T standard process 1P5M by the Taiwan Semiconductor Manufacturing Company, Limited (TSMC) were in the state of bonding pad opening for later NPL integration. Each 8" wafer contained 55 functional dies, and the die number was labeled to track the performance as shown in Supplementary Fig. S1(a). Eight parameters (four pinhole sizes with and without color filter (CF)) were split in each sensor die, and the pixel coordinates were assigned from R0C0 to R255C255 from the upper left to the lower right corner (Supplementary Fig. S1(b)). The cross-section of the grating and pixel area of the incoming TPD CMOS sensor is shown in Supplementary Fig. S1(c). From R0C0 to R0C177, a FUJIFILM color filter (SYS-A721A, FUJIFILM Electronic Materials Co., Ltd., Taiwan) with a thickness of 0.5 μm and a square area of 12x12 μm^2 was lithographically patterned by an 8" aligner (ABM Mask Aligner System, AB-M, Inc., Germany) with ~1-μm alignment accuracy to the pixel center. To avoid peeling, the color filter micropattern was fully crosslinked at 200°C for 2 hr before SiO_2 deposition for chemical mechanical polishing (CMP) planarization (Supplementary Fig. S1(d)). The surface profile and roughness were measured by a surface profiler (Dektak XTL Profiler, Bruker, USA) and an

atomic force microscope (AFM) (Dimension 3100, Digital Instruments (DI), Veeco, USA or JPK Instrument NanoWizard, JPK Instruments AG, Germany). The step height and SiO_2 average roughness (***Ra***) were controlled to less than 20 nm and 0.5 nm, respectively, after this procedure following the CMP planarization processes. As shown in Supplementary Fig. S1(e), the wafer was deposited with a 550-nm longpass interference filter and a Ti metal layer at 300°C through a shadow mask. The opening square of the shadow mask on each die is indicated by the red dotted line in Supplementary Fig. S1(b). The shadow area protected the alignment marks from covering the opaque Ti metal such that later photolithography alignment could proceed.

Four sizes of pinholes were fabricated through DUV photolithography (FPA-5000 ES4 248 nm KrF Scanner, Canon, Japan) on a 0.8-μm photoresist (PR) YSB663 (Nippon Zeon Co., Ltd., Japan) with a bottom anti-reflection coating (BARC) of 60-nm AR3™-600 (Dow® Electronic Materials, USA). AMAT DPS II etching (DPSII Centura® etcher, Applied Materials, USA) was performed at an RF power of 500/85 W, a chamber temperature of 80°C, a chamber pressure of 5 mTorr, a $BCl_3/Cl_2/Ar$ flow rate of 30/25/60 sccm, and an etching time of 300 sec. The wafer was then deposited with SiO_2 at 300°C and submitted to CMP (Supplementary Fig. S1(f)). $Al_2O_3/Ta_2O_5/SiO_2$ (selective modification layer/core layer/lower cladding) layers with thicknesses of 20 nm/150 nm/~700 nm were deposited at 300°C through the shadow mask (Supplementary Fig. S1(g)). A grating nanostructure with a period of 280 nm and a 50% duty cycle was fabricated (outside the pixel array area of each die and in the green area in Supplementary Fig. S1(b)) by DUV photolithography on 170-nm photoresist GKR-5201 (FUJIFILM Electronic Materials Co., Ltd., Japan) with 55-nm DUV-42 (Brewer Science Inc., USA) and two-step AMAT DPSII etching. The first etching was performed to etch through the Al_2O_3 layer at an RF power of 500/85 W, a chamber temperature of 80°C, a chamber pressure of 5 mTorr, a $BCl_3/Cl_2/Ar$ flow rate of 30/25/60 sccm, and an etching time of 60 sec. The second etching was performed to remove the Ta_2O_5 layer at an RF power of 1600/50 W, a chamber temperature of 80°C, a chamber pressure of 10 mTorr, a $Cl_2/N_2/CHF_3$ flow rate of 60/25/15 sccm, and an etching time of 30 sec (Supplementary Fig. S1(h)).

A nanopillar array of PR/BARC was fabricated by DUV photolithography on 600-nm YSB-663/60-nm AR3™-600, with LAM 9100 etching (Lam A9100 oxide etcher, Lam Research, USA) performed at an RF power of 800/100 W, a chamber pressure of 3 mTorr, a N_2/O_2 flow rate of 35/5 sccm, and an etching time of 24 sec. Then, a SiO_2 layer was deposited on the wafer at 150°C as the upper cladding and submitted to CMP (Supplementary Fig. S1(i)). Two thin layers of 30-nm SiO_2/60-nm Ti were deposited on the wafers at 150°C *via* the shadow mask (Supplementary Fig. S1(j)).

An array of larger holes with a diameter of 700 nm was patterned on the PR/BARC nanopillar array through DUV photolithography on 600-nm YSB-663 photoresist with 60-nm AR3™-600. First, AMAT DPSII etching was performed at an RF power of 500/120 W, a chamber pressure of 6 mTorr, an $N_2/CF_4/CHF_3$ flow rate of 30/10/40 sccm, and an etching time of 245 sec to remove 60 nm of Ti and a certain thickness of SiO_2 until the PR/BARC nanopillar was revealed. In addition, the SiO_2/Ti layers on the grating area were removed for laser light coupling. Then, AMAT DPSII ashing (in an advanced strip passivation (ASP) chamber) for PR/BARC nanopillar removal was performed at an RF power of 2500 W, a chamber temperature of 180°C, a chamber pressure of 2000 mTorr, a N_2/O_2 flow rate of 400/1500 sccm, and an etching time of 600 sec. The PR/BARC nanopillar served as a sacrificial nanostructure for the formation of a T-shaped nanowell. Because the ashing process only removes PR/BARC (or other organic materials), the nanowell bottom could be precisely controlled on the top surface of the Al_2O_3 (as an etching stop) without any damage to the Al_2O_3 or Ta_2O_5 layer on the entire 8" wafer (Supplementary Fig. S1(k)). Unless indicated otherwise, in the abovementioned processes, DUV photolithography provided an alignment accuracy of less than 80 nm between any two adjacent layers.

2. NPL design principle

To investigate optical phenomena without cross-talk among neighboring pixels, the pitch of the pixel array in the TPD CMOS wafer was designed to be 50 μm, and the pixel size was 10x10 μm^2, with an

opening of the same size on the top metal. The purpose of NPLs is to generate a sufficient signal-to-noise ratio to collect adequate fluorescence signals from a reaction site and to block as much excitation light as possible. The optical density (OD) of a total internal fluorescence microscope (TIRFM) is usually 8-10 for single-molecule detection;[1,2] therefore, the nanostructures designed for reducing the excitation light wavelength were assumed to possess the same OD values of ~9. Three nanodevices for reducing excitation scattering were employed in the NPLs: (1) a metal pinhole to prevent most of the scattering light from entering the sensor pixel; (2) an interference filter to dissipate the amplitude of the excitation scattering by the deposition of multiple layers of two materials, such as Ta_2O_5 (n=2.16) and SiO_2 (n=1.46); and (3) a color filter to absorb the scattering energy.

Considering the efficiency of the collection signal from the nanowell to a 10x10-μm^2 TPD pixel and the light diffraction limit, the sizes of the openings of the metal pinhole should be approximately 2 μm. The real fabricated nanostructures had a geometric deviation and misalignment of ~80 nm between any two structures of the nanowell, the metal pinhole, and the top metal opening in the TPD CMOS. Therefore, to effectively optimize the integration parameters and also tolerate fabrication variations, pinholes measuring ø1.0 μm, ø1.5 μm, ø2.0 μm, and ø2.5 μm were arranged in the NPLs.

Due to the opaque shielding of the Ti metal, very little scattering light can pass through the pinhole layer. Therefore, the metal pinhole contributes a certain OD. The four sizes of the pinholes, ø1.0 μm (OD 3.4), ø1.5 μm (OD 3.0), ø2.0 μm (OD 2.8), and ø2.5 μm (OD 2.6), confine the cone angles of the collection light from the nanowells to the TPD detectors. The collected light spot/cone angles ($\boldsymbol{\alpha}$) were ø6 μm/32° (±16°), ø10 μm/51° (±25.5°), and ø14.3 μm/69° (±34.5°) *via* pinhole sizes of ø1.0 μm, ø1.5 μm, and ø2.0 μm, respectively. For the ø2.5-μm pinhole, emission light at a cone angle of less than 82° (±41°) can pass through the pinhole. However, the top metal shielding with a square 10x10-μm^2 opening on top of each pixel in the TPD CMOS wafer further blocks some of the light (see Supplementary Fig. S1(l)).

Because the ideal pinhole size was determined to be ø2 μm (the entire pixel is perfectly covered

by the emission light from the bottom of the nanowell, as shown in Supplementary Fig. S1(l)), the total depth from the bottom of the metal pinhole to the top surface of the pixel was defined, as was the emission light coverage area on the pixels *via* the other pinhole sizes. The upper and lower claddings of the SiO_2 layer were assigned to be at least 500 nm thick to prevent Ti from absorbing the light intensity from the core layer of the Ta_2O_5 waveguide. Thus, a maximum thickness of 4.2 μm could be used between the metal pinhole and the TPD CMOS wafer for the interference and color filters.

The OD of the Ta_2O_5/SiO_2 longpass interference filter can be designed to be OD 2.2 with a thickness of 1.4 μm or OD 4.8 with a thickness of 2.6 μm at an incident angle of 0° (the incident light path is perpendicular to the substrate). Although a 4.2-μm interference filter (plus a ø2-μm pinhole) can contribute an OD of ~7 (~10) at an incident angle of ±30°, the OD decreased rapidly with increasing incident angle. Consequently, an absorption filter of a certain thickness was utilized under the interference filter to further remove the excitation scattering at a larger incident angle (the color filter must be located underneath the interference filter to minimize autofluorescence and peeling). The thicknesses of the color filter and interference filter were thus set to 0.5 μm for an OD of ~1 and to 2.6 μm for an OD of ~5 at a blue excitation wavelength, respectively (Supplementary Fig. S2).

The excitation light scattering originated from (1) incident laser collision at the grating coupler; (2) nanowell structure-induced waveguide scattering; and (3) roughness-induced waveguide scattering between the upper and lower Ta_2O_5-SiO_2 interfaces. The 0.3-μm Ti metal layer under the grating area reflected most of the incident laser energy (only less than 10^{-10} laser intensity can transmit through the metal layer), which can significantly reduce the noise disturbance derived from the excitation light. The majority of the scattering energy then propagates between the upper and lower cladding layers; thus, a Ti material with ~40% absorption was selected and arranged on the upper cladding (60 nm) and under the lower cladding (0.3 μm) layers to dissipate the scattering energy propagating between the upper and lower cladding layers.

The components contributing to the total OD for a 473-nm wavelength were as follows: (1)

metal pinholes that provided ODs of 3.4, 3.0, 2.8, and 2.6 for ø1.0 μm, ø1.5 μm, ø2.0 μm, and ø2.5 μm, respectively; (2) interference filters that contributed ODs of 4.8, 4.4, and 3.8 at incident angles of ±16° and ±25.5°, ±34.5°, and ±41°, respectively (Supplementary Fig. S2(d)); and (3) a color filter that provided an OD of 1.1. The ideal pinhole measuring ø2.0 μm was sufficient to collect the maximum emission signals from the nanowells and to block 473-nm scattering after the NPL with the color filter (OD 8.3). The remainder of the combinations had a minimum OD of 6.4 and a maximum OD of 9.3.

3. Filters on TPD CMOS

To clarify the filter effect, the response curve was measured by covering the normal TPD CMOS with an interference filter alone, a color filter alone, or an interference filter plus a color filter (Supplementary Fig. S3(e)-(g)). The response curve approximately matched the transmittance spectrum except for the wavelength slope between 450 and 550 nm for the interference filter (Supplementary Fig. S3(e)) and the wavelength slope between 400 and 500 nm for the color filter (Supplementary Fig. S3(f)) on the TPD CMOS sensor. The former inconsistency occurred because the incident angles of the exposure light on the TPD CMOS were random from the outlet of the integrated sphere. The interference filter was invalid for incident light angles larger than a certain degree (Supplementary Fig. S2(d)); thus, the overall OD of the interference filter decreased from 450 to 550 nm. The latter inconsistency was due to the high autofluorescence of the color filter at the absorption wavelength. Therefore, the emitted fluorescence of a longer wavelength contributed a strong signal intensity at each junction. Considering the properties of both filters, the stacking interference filter on top of the color filter can effectively block most of the incident light at a valid angle through the interference filter, absorb the remainder of the incident light at a large angle through the color filter, and cause little autofluorescence from the color filter. However, it is not appropriate to place the color filter on top of the interference filter because the longer wavelength of the autofluorescence from the color filter can transmit through the interference filter to affect the

sensing signals.

4. Photon collection after the pinhole

The light collection intensity of the TPD detector before and after filter deposition or NPL integration was measured by exposing TPD CMOS sensors to 590-nm light from a Mightex BioLED system at 49 nW/cm^2, which represents 150 ph/(pixel·ms) for the normal TPD CMOS (Supplementary Fig. S4 (a)). Then, the filter transmittance was measured under the same intensity to compare the transmittances of various filter combinations (Supplementary Fig. S4 (b)-(d)). The BioLED intensity was measured by a power meter (PD300, Ophir Optronics Solutions Ltd., Germany), and the pixel for the normal TPD CMOS or normal TPD CMOS plus filter(s) was R100C100.

Because the metal pinholes blocked most of the light and decreased the illumination flux from the light source to the TPD detector, the exposure light powers for the four pinhole openings with or without a color filter on the NPL-integrated TPD CMOS were adjusted to obtain similar signal intensities (Supplementary Fig. S4 (e)-(l)) to study the ODs of the pinhole sizes. More precisely, the power of the 590-nm LED light was calibrated, using the PD300 power meter, to the intensity that occurred when the NPL-integrated TPD without a color filter (as shown in Supplementary Fig. S4 (i)-(l)) had a similar signal response to the normal TPD plus interference filter (as shown in Supplementary Fig. S4 (b)) for each pinhole size.

The 8 pixels of the NPL-integrated TPD CMOS were R50C106, R92C106, R156C106, R200C106, R50C184, R92C184, R156C184, and R200C184 for the ø1.0-μm pinhole with a color filter, the ø1.5-μm pinhole with a color filter, the ø2.0-μm with a color filter, the ø2.5-μm pinhole with a color filter, the ø1.0-μm without a color filter, the ø1.5-μm pinhole without a color filter, the ø2.0-μm pinhole without a color filter, and the ø2.5-μm pinhole without a color filter, respectively.

The photon collection intensity of the TPD detector was calculated by subtracting the average of 100 continued dark values from the average of 100 continued signal values for each junction from one pixel under each condition. The linearities of the signal intensity, dark intensity, and signal minus

dark intensity were measured over integration times ranging from 25 ms to the longest integration time before saturation of the signal intensity.

The four BioLED light spectra are shown in Supplementary Fig. S4(m). The ratio of the 590-nm BioLED intensity for the four pinhole openings compared to that for the normal TPD can be converted to the ODs of the metal pinholes: 2.5×10^{-4} (OD 3.6), 4.4×10^{-4} (OD 3.4), 17.9×10^{-4} (OD 2.8), and 36.8×10^{-4} (OD 2.4). The light collection ratio roughly matched the design that was proportional to the opening area over the overall area (Supplementary Fig. S4(n)).

References

1. Erdogan, T. Optical Filters for Wavelength Selection in Fluorescence Instrumentation. *Curr. Protoc. Cytom.* **2011**, *56*, 2.4.1-2.4.25.
2. Wazawa, T.; Ueda, M. Total Internal Reflection Fluorescence Microscopy in Single Molecule Nanobioscience. *Adv. Biochem. Eng. Biotechnol.* **2005**, *95*, 77–106.

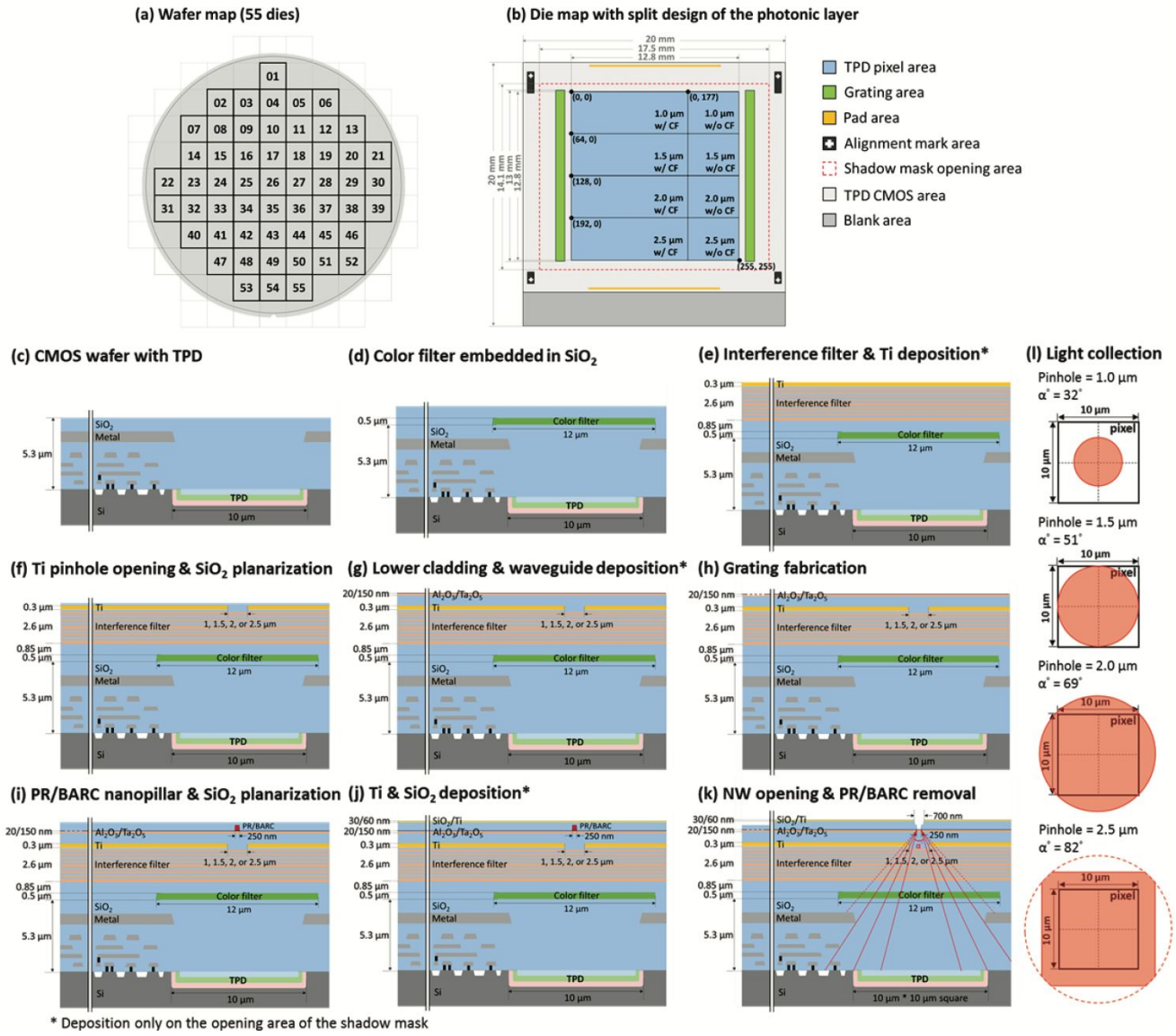

Fig. S1 Wafer/die map of the NPL-integrated TPD CMOS and the fabrication flow. (a) Wafer map of the 8" TPD CMOS wafer. (b) Die map with NPL integration fabricated only on the TPD sensor inside the shadow mask opening area (red dashed line). The color filter is arranged from R0C0 to R255C177. The Ti pinhole opening has four sizes: ø1 µm from R0C0 to R63C255; ø1.5 µm from R64C0 to R127C255; ø2 µm from R128C0 to R191C255; and ø2.5 µm from R192C0 to R255C255. (c) The incoming TPD CMOS sensor chips are in 8" wafers. (d) The color filter covers an area of 12x12 μm^2 on the pixel area from R0C0 to R255C177 that is photolithographically formed by an 8" aligner with 365-nm UV exposure light in the TPD area; the filter is then embedded in SiO_2 and submitted to CMP. (e) The wafer is covered with a 40-layer interference filter by alternating Ta_2O_5/SiO_2 deposition and a layer of Ti metal. (f) Four sizes of Ti pinholes are patterned by DUV photolithography with 248-nm KrF light and dry etched through the Ti layer. The pinholes are refilled by SiO_2 and submitted to CMP. (g) A lower cladding of 550-nm SiO_2, a core layer of 150-nm Ta_2O_5 as a waveguide, and a surface modification layer of 20-nm Al_2O_3 are sequentially deposited on the wafer. (h) The grating structure is patterned by DUV photolithography and dry etched. (i) The PR/BARC nanopillar array on the pixel area is defined by DUV photolithography and then embedded with a SiO_2 upper cladding layer polished by CMP. (j) Thin layers of 60-nm Ti and 30-nm SiO_2 are deposited to block light scattering from the waveguide. (k) A ø700-nm nanowell array on the ø250-nm nanopillar array is patterned and dry etched to reveal the nanopillar. The PR/BARC nanopillar is then removed by O_2/Ar plasma to form a T-shaped nanowell array with an undamaged Al_2O_3 bottom surface. In addition, the thin layers of Ti and SiO_2 on top of the grating area are removed for laser coupling into the Ta_2O_5 planar waveguide. (l) Emission light collection angle, α°, through the four pinhole sizes: 32° for ø1.0-µm, 51° for ø1.5-µm, 69° for ø2.0-µm, and 82° for ø2.5-µm pinholes.

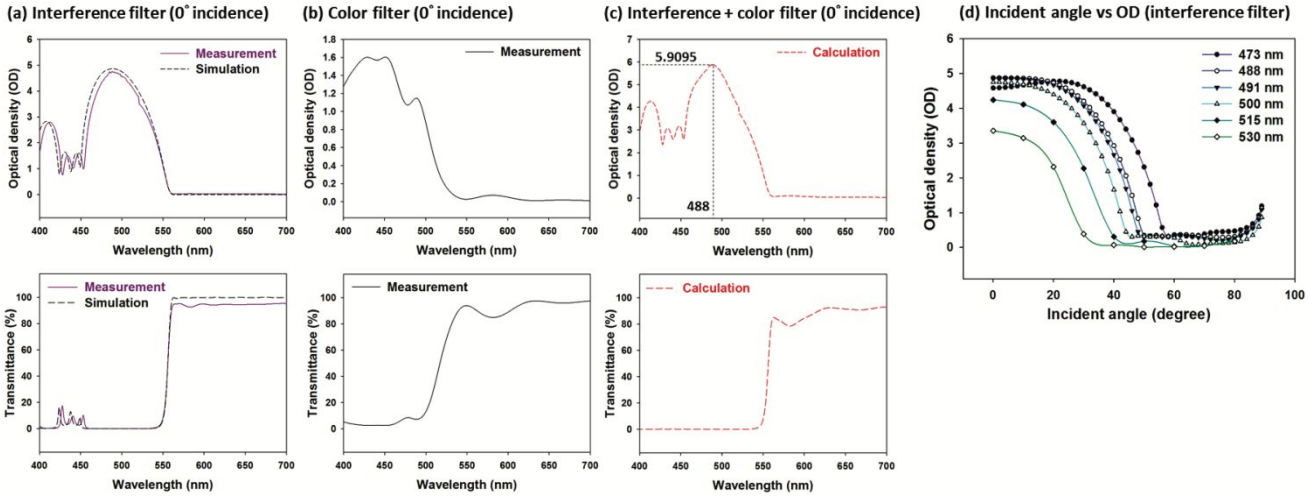

Fig. S2 Spectra of the interference filters and color filters. (a) Spectra of the 2.6-μm Ta_2O_5/SiO_2 interference filter determined by simulation (black dashed line) and measurement (purple line). (b) Spectra of the 0.5-μm FUJIFILM color filter determined by measurement (black line). (c) Spectra of the interference filter plus the color filter (red dashed line) determined by directly multiplying the measured transmittance spectra of the interference filter and color filter. (d) Optical density (OD) simulated over incident angles of 0° to 90°and various wavelengths.

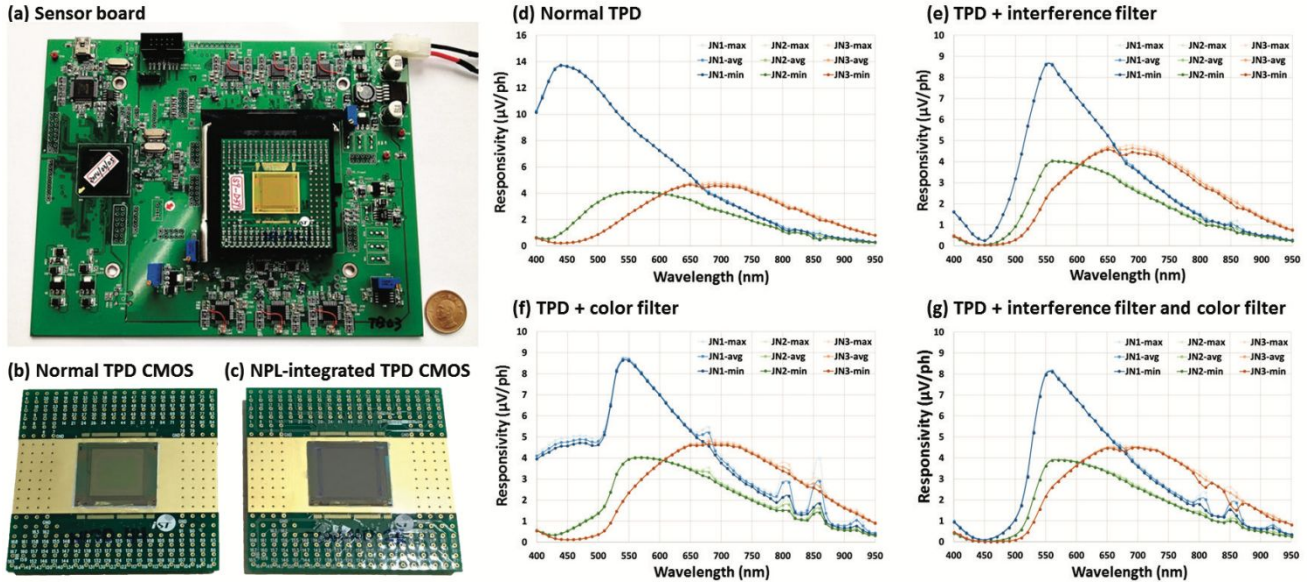

Fig. S3 TPD CMOS sensor/board and response curves. (a) Sensor board for collecting TPD CMOS data. Photographs of wire-bond packaged (b) normal TPD CMOS and (c) NPL-integrated TPD CMOS. Response curves of TPD before and after filter(s) integration: (d) normal TPD, (e) only interference filter on the TPD, (f) only color filter on the TPD, and (g) both interference filter and color filter on the TPD.

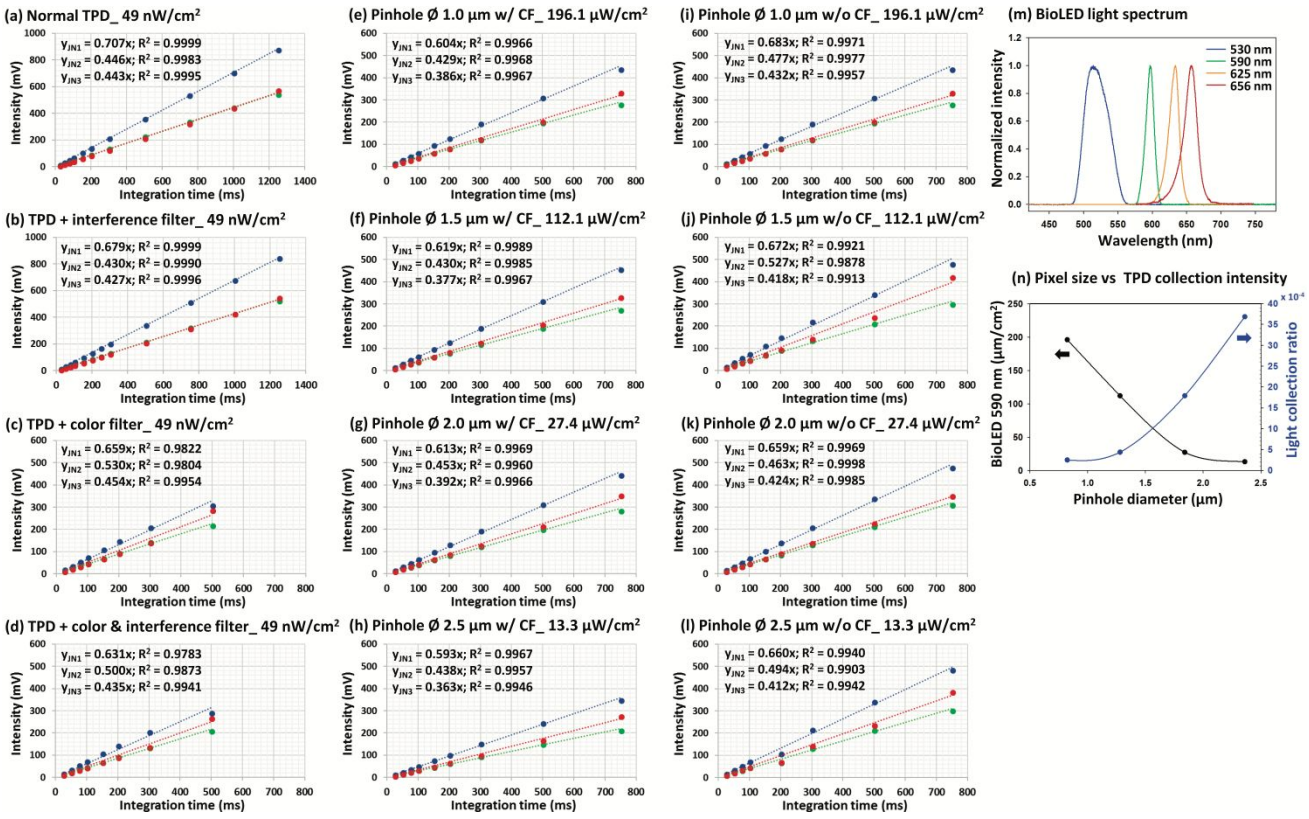

Fig. S4 Linearity between integration time and TPD CMOS responsive intensity and light collection ratio through pinhole opening diameters. For comparison of the filter transmission, the 590-nm BioLED light at 49 nW/cm^2 was illuminated on (a) the normal TPD CMOS, (b) the TPD CMOS with only an interference filter, (c) the TPD CMOS with only a color filter, and (d) the TPD CMOS with both an interference filter and a color filter (but without other NPLs). (e)-(l) After NPL integration, the 590-nm BioLED intensity was adjusted to the intensity that occurred when the TPD with each pinhole size in the integrated CMOS had the same signal response as the normal TPD. (m) Normalized artificial BioLED light spectrum. (n) Light collection ratio after metal pinholes of four different sizes on the NPL-integrated TPD CMOS (compared to the normal TPD).

Tab. S1 Normal TPD CMOS decoding data under (a) fixed and (b) random pulses/intervals. Note: All the integration times are fixed at 25 ms.

(a) Fixed pulse/interval length									
illumination intensity		Pulse (ms)	100	150	200	250	300	350	500
		Interval (ms)	100	150	200	250	300	350	500
ph/pixel·ms (ph/pixel·data)	150/100/150/100 (3750/2500/3750/2500)	# of 530/590/625/656	26/24/20/30	29/27/21/23	25/27/27/21	26/24/31/19	19/28/31/22	22/22/27/29	24/20/29/27
		# of correct segment pixels	46	52	51	46	44	45	48
		# of correct decoding pixels	1	20	31	31	30	31	38
	175/125/175/125 (4375/3125/4375/3125)	# of 530/590/625/656	19/27/36/18	26/20/25/29	26/21/28/25	23/29/24/24	26/31/23/20	25/28/23/24	22/23/27/28
		# of correct segment pixels	53	56	59	51	53	51	52
		# of correct decoding pixels	0	47	57	50	52	50	51

(b) Random pulse/interval length					
			No.1	No.2	No.3
illumination intensity		Pulse (ms)	150 ~ 500		
		Interval (ms)	200 ~ 5000		
ph/pixel·ms (ph/pixel·data)	175/125/175/125 (4375/3125/4375/3125)	# of 530/590/625/656	36/19/26/19	26/20/24/30	22/34/24/20
		# of correct segment pixels	49	52	47
		# of correct decoding pixels	48	51	47

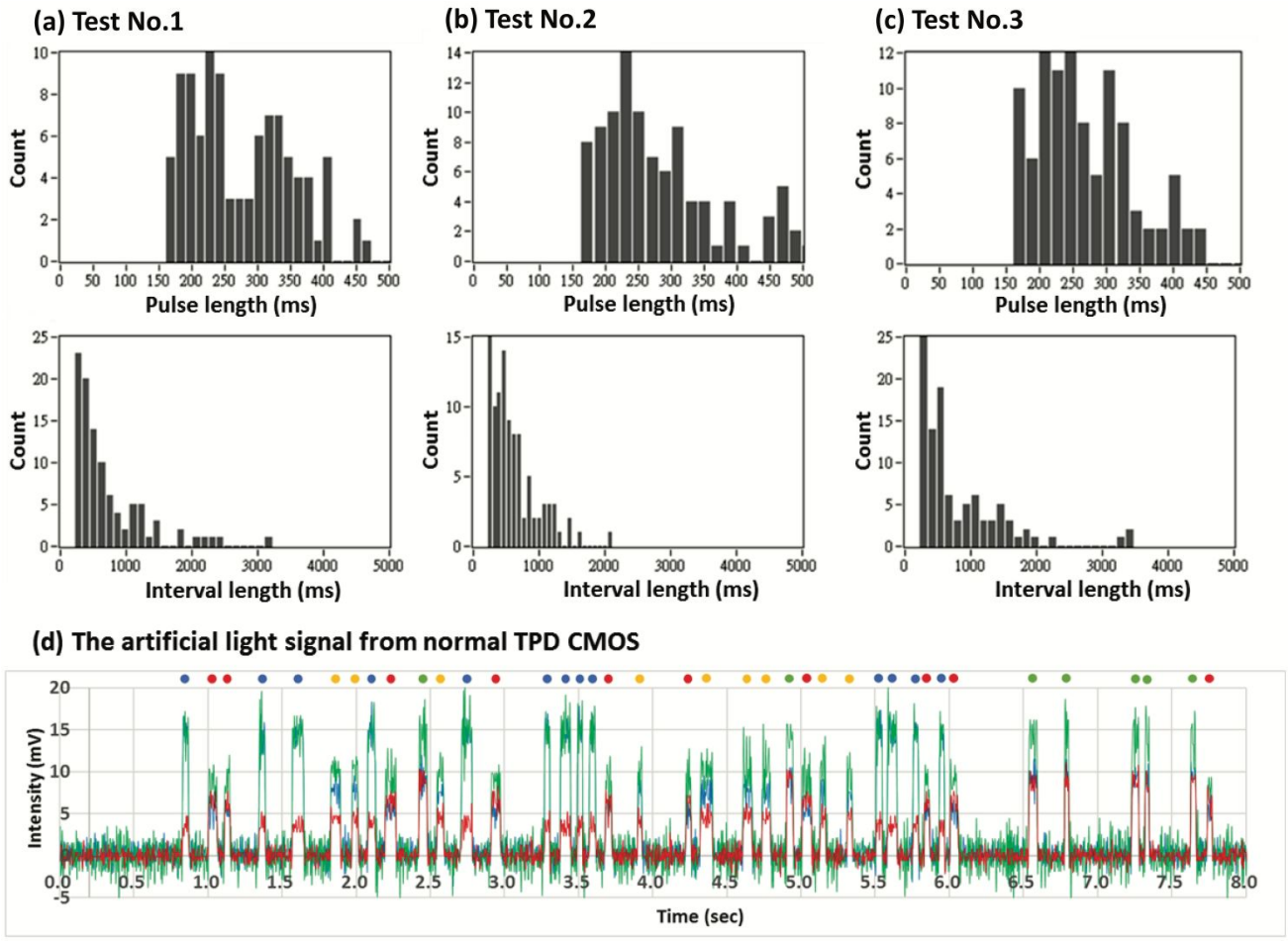

Fig. S5 BioLED illumination histograms and normal TPD detection signals. Histograms of 100 random pulse and interval lengths of (a) test No. 1, (b) test No. 2, and (c) test No. 3. (d) A portion of the artificial light signals from the normal TPD from test No. 1. Blue/green/yellow/red represent BioLED signals of 530/590/625/656 nm.

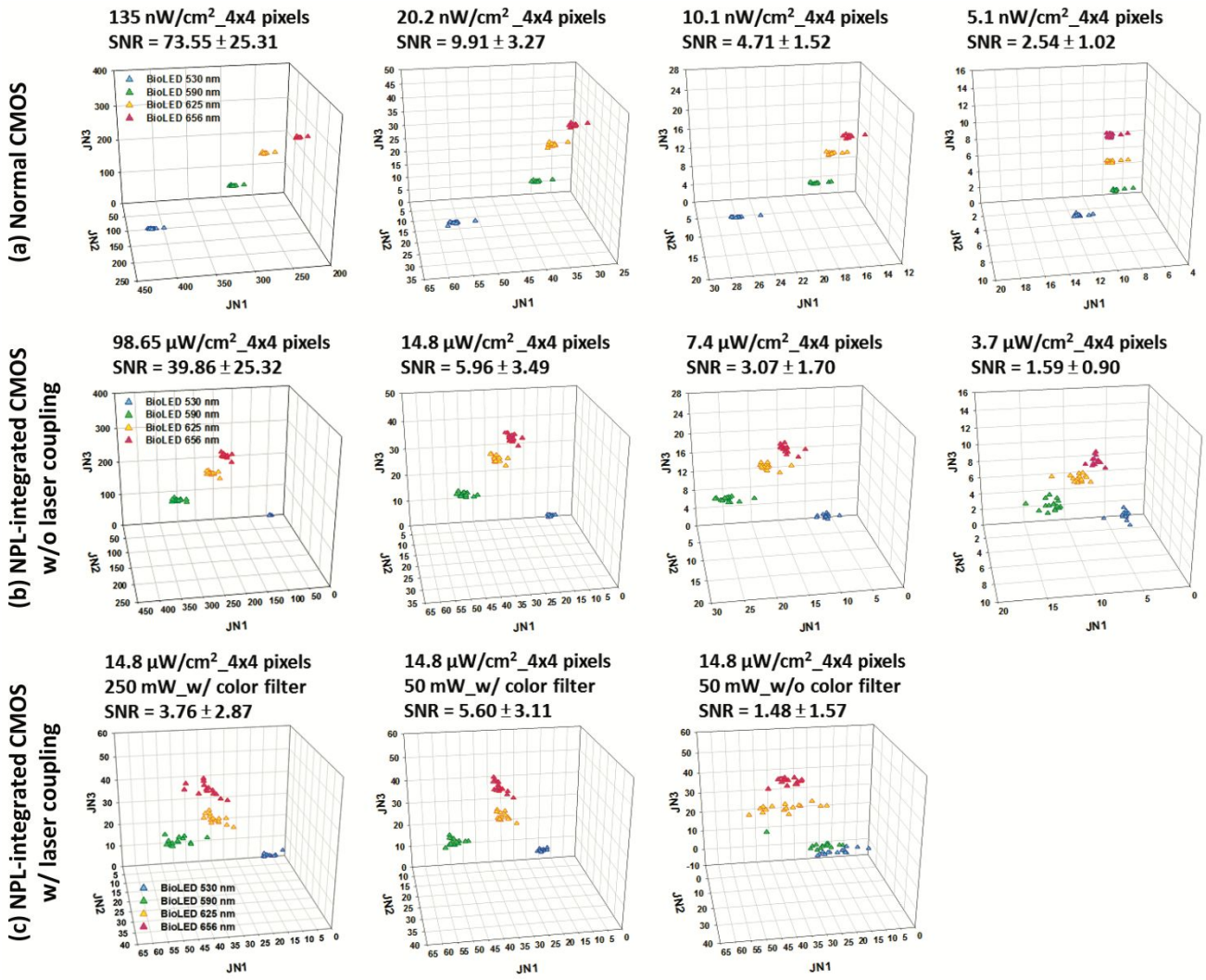

Fig. S6 Three-dimensional junction maps from 4x4 pixels (average of 100 data points for a pixel) for the comparison of pixel variation. (a) Normal TPD CMOS: the signal junction map presents the distinct identities of four BioLED lights under illumination intensities of 135, 20.2, 10.1, and 5.1 nW/cm^2, which represent 75000, 11250, 5625, and 2813 photons, respectively, collected by each pixel under a 150-ms integration time. (b) NPL-integrated TPD CMOS in the region with a ø2.0-µm pinhole and a color filter and without laser coupling: the illumination intensities of 96.65, 14.8, 7.4, and 3.7 µW/cm^2 represent ~1.3 times the photon collection for the normal TPD CMOS. (c) NPL-integrated TPD CMOS in the region with a ø2.0-µm pinhole and 473-nm laser coupling. (All axis units: mV)

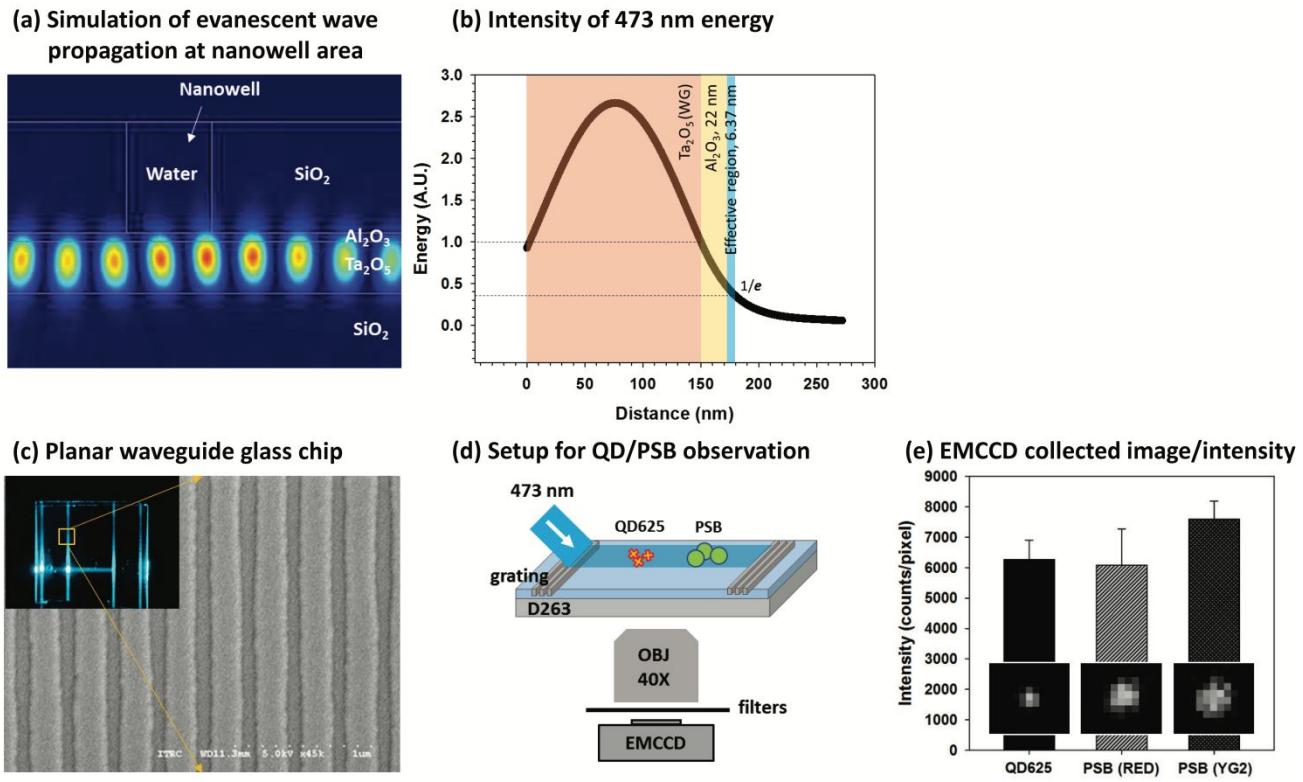

Fig. S7 Evanescent wave intensity distribution in the nanowell area of the NPL-integrated TPD CMOS and QD/PSB emission intensity comparison on a commercial microscope. (a) Simulation plot and (b) 473-nm intensity profile in the planar waveguide in the nanowell area. The effective region is at the height of the nanowell with an intensity greater than 1/***e*** from the surface of the planar waveguide. Because the evanescent wave can only excite the fluorescent molecules in the effective region, (c) a commercial planar waveguide glass chip with similar grating and waveguide specifications is used on (d) a microscope setup for (e) EMCCD image/intensity comparison between the single molecules of QDs and PSBs.

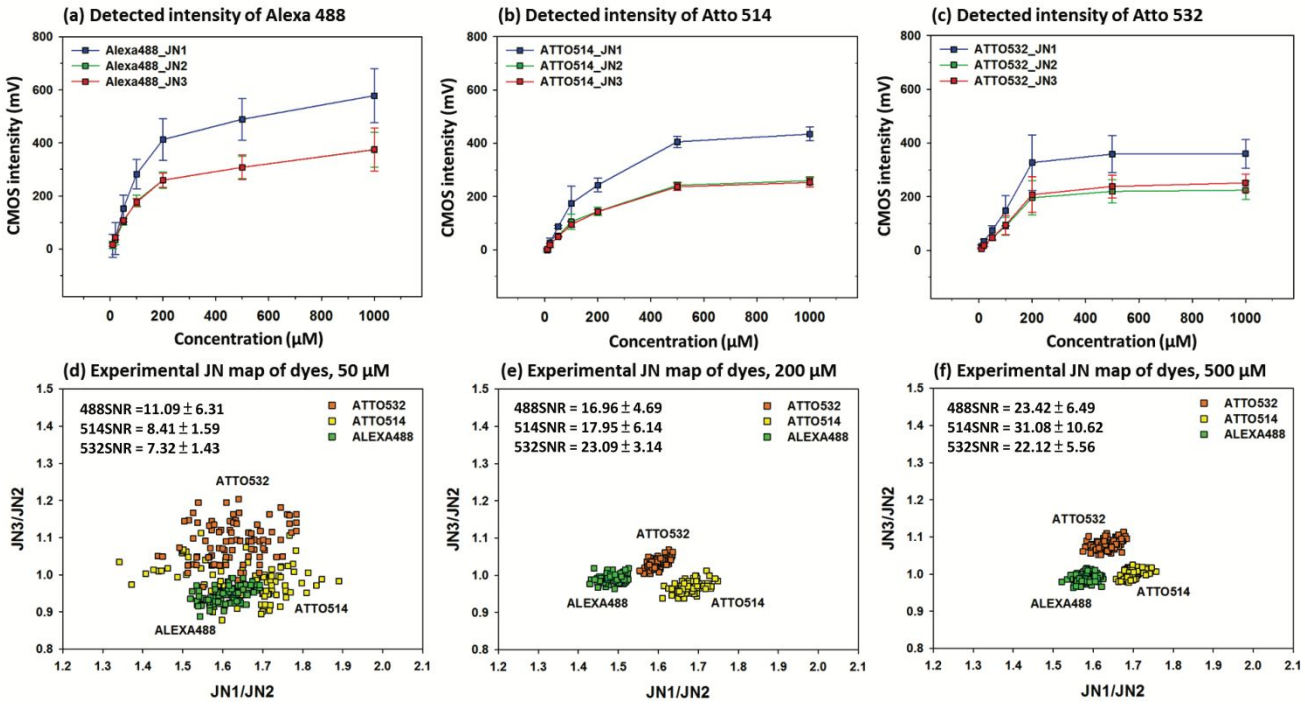

Fig. S8 Integrated TPD CMOS intensities of series dilutions of three fluorescent dyes. TPD CMOS intensity curves of (a) Alexa 488, (b) Atto 514, and (c) Atto 532 at concentrations from 10 μM to 1 mM. Experimental 2D junction maps of fluorescent dyes at concentrations of (d) 50 μM, (e) 200 μM, and (f) 500 μM.

Tab. S2 TPD Detection intensities of three fluorescent dyes and estimated minimum dye numbers for a reliable SNR.

	NPL-integrated TPD CMOS									TIRFM EMCCD
	Signal-background intensity (mV/μM)			Peak-to-peak noise variation (mV)		Min. concentration for SNR=3 (μM)		Min. dye numbers for SNR=3*		Relative intensity
		@150 ms	@50 ms	@150 ms	@50 ms	@150 ms	@50 ms	@150 ms	@50 ms	(A.U.)
QD625										1.000
Alexa 488	JN1	2.828	0.943	6.917	4.462	7.338	14.200	0.96	1.94	0.196± 0.020
	JN2	1.845	0.615	5.012	3.426	8.150	16.715			
	JN3	1.845	0.615	3.914	2.667	6.364	13.007			
Atto 514	JN1	1.712	0.571	6.917	4.462	12.124	23.461	1.73	3.49	0.187± 0.021
	JN2	1.022	0.341	5.012	3.426	14.710	30.171			
	JN3	0.945	0.315	3.914	2.667	12.422	25.389			
Atto 532	JN1	1.597	0.532	6.917	4.462	12.993	25.143	1.78	3.57	0.224± 0.036
	JN2	0.960	0.320	5.012	3.426	15.662	32.123			
	JN3	1.013	0.338	3.914	2.667	11.597	23.704			

*Assume the effective region is 6.37 nm where the excitation intensity decays to 1/***e** compared to the waveguide surface.

Movie S1 A 473-nm line laser coupling into the planar waveguide through the left grating of the NPL-integrated TPD CMOS. First, an incident angle of 3.7° is fixed, and a lateral displacement is performed. Then, the coupling angle is adjusted back and forth to observe the coupling efficiency. Note: row numbers 0-30 and 228-255 are in the defect area.